Dieses Dokument ist eine Zweitveröffentlichung (Postprint) /

This is a self-archiving document (accepted version):

Franz P. G. Fengler, Robin Nigon, Paul Muralt, Everett D. Grimley, Xiahan Sang, Violetta Sessi, Rico Hentschel, James M. LeBeau, Thomas Mikolajick, Uwe Schroeder

Analysis of Performance Instabilities of Hafnia-Based Ferroelectrics Using Modulus Spectroscopy and Thermally Stimulated Depolarization Currents

Erstveröffentlichung in / First published in:

Advanced electronic materials. 2018, 4(3), Art.-Nr.1700547 [Zugriff am: 24.08.2022]. Wiley. ISSN 2199-160X.

DOI: https://doi.org/10.1002/aelm.201700547

Diese Version ist verfügbar / This version is available on:

https://nbn-resolving.org/urn:nbn:de:bsz:14-qucosa2-804969

SLUB
Wir führen Wissen.

TECHNISCHE UNIVERSITÄT DRESDEN

QUCOSA Quality Content of Saxony

Final edited form was published in "Advanced electronic materials". 2018, 4(3), Art.-Nr. 1700547. ISSN 2199-160X.
https://doi.org/10.1002/aelm.201700547

Analysis of Performance Instabilities of Hafnia-Based Ferroelectrics Using Modulus Spectroscopy and Thermally Stimulated Depolarization Currents

*Franz P. G. Fengler, Robin Nigon, Paul Muralt, Everett D. Grimley, Xiahan Sang, Violetta Sessi, Rico Hentschel, James M. LeBeau, Thomas Mikolajick, and Uwe Schroeder**

The discovery of the ferroelectric orthorhombic phase in doped hafnia films has sparked immense research efforts. Presently, a major obstacle for hafnia's use in high-endurance memory applications like nonvolatile random-access memories is its unstable ferroelectric response during field cycling. Different mechanisms are proposed to explain this instability including field-induced phase change, electron trapping, and oxygen vacancy diffusion. However, none of these is able to fully explain the complete behavior and interdependencies of these phenomena. Up to now, no complete root cause for fatigue, wake-up, and imprint effects is presented. In this study, the first evidence for the presence of singly and doubly positively charged oxygen vacancies in hafnia–zirconia films using thermally stimulated currents and impedance spectroscopy is presented. Moreover, it is shown that interaction of these defects with electrons at the interfaces to the electrodes may cause the observed instability of the ferroelectric performance.

1. Introduction

The recent discovery of ferroelectricity in thin doped hafnia films might enable ferroelectric random-access memory (FeRAM) to become one viable candidate for future memory solutions. Similar to a dynamic random-access memory (DRAM), the memory cell of an FeRAM consists of a dielectric sandwiched between two metal electrodes. However, unlike the dielectric in a DRAM cell which loses its polarization after removal of an electric field, the ferroelectric in the FeRAM cell preserves a bistable polarization orientation following field removal. These two bistable states can be switched from one to the other within nanoseconds by application of an electric field above the coercive field.[1] Commercial ferroelectric memories possess endurances of up to 10^{14} cycles[2] while allowing for a low-power write consumption, which is unachievable with any other nonvolatile memory technology so far.[3] The most common ferroelectrics are perovskites like lead zirconate titanate (PZT). Traditional perovskite ferroelectrics often suffer from integration issues which hinder further downscaling and are only meaningful in niche applications where the low write energy is essential or as embedded memory in logic large-scale integration circuits.[3] In contrast, hafnium oxide has been a standard material in complementary metal oxide semiconductor (CMOS) production for around a decade.[4] The recent discovery of ferroelectricity in thin doped hafnia films is poised to solve the scaling issues of conventional perovskite-based FeRAM. Various dopants, e.g., Si,[5] Gd,[6] La,[7] Sr,[8] Al,[9] and Y[10] are known to stabilize the orthorhombic polar $Pca2_1$ phase in hafnia.[11] Of all compositions so far, a mixture of equal parts of hafnia and zirconia enables the widest known process window within this family of ferroelectrics. This composition maintains full process compatibility with the CMOS technology.[12] Both oxides are already used in high-*k* metal gate[4] and DRAM[13] processes and can be deposited by the well-developed atomic layer deposition (ALD) technique. This allows conformal depositions onto 3D structures for state-of-the-art technology nodes.[14]

The technological breakthrough of HfO_2-based FeRAM, however, is hindered by its high coercive field which requires a high operation voltage and by its unstable ferroelectric performance. During electric field cycling, an initial increase of the remnant polarization—the so-called wake-up behavior—is often observed. This is connected to the reduction of an internal field

F. P. G. Fengler, R. Hentschel, U. Schroeder
NaMLab gGmbH
Noethnitzer Str. 64, Dresden D-01187, Germany
E-mail: Uwe.Schroeder@namlab.com

R. Nigon, P. Muralt
Laboratoire de Céramique
EPFL, MX-D Ecublens
1015 Lausanne, Switzerland

E. D. Grimley, J. M. LeBeau
Department of Materials Science and Engineering
North Carolina State University
Raleigh, NC 27695-7907, USA

X. Sang
Center for Nanophase Materials Sciences
Oak Ridge National Laboratory
Oak Ridge, TN 37831, USA

V. Sessi, T. Mikolajick
Chair of Nanoelectronic Materials
TU Dresden, D-01062, Dresden, Germany

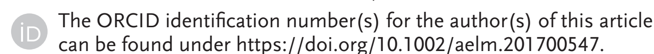
The ORCID identification number(s) for the author(s) of this article can be found under https://doi.org/10.1002/aelm.201700547.

Provided by Sächsische Landesbibliothek - Staats- und Universitätsbibliothek Dresden

Final edited form was published in "Advanced electronic materials". 2018, 4(3), Art.-Nr. 1700547. ISSN 2199-160X.
https://doi.org/10.1002/aelm.201700547

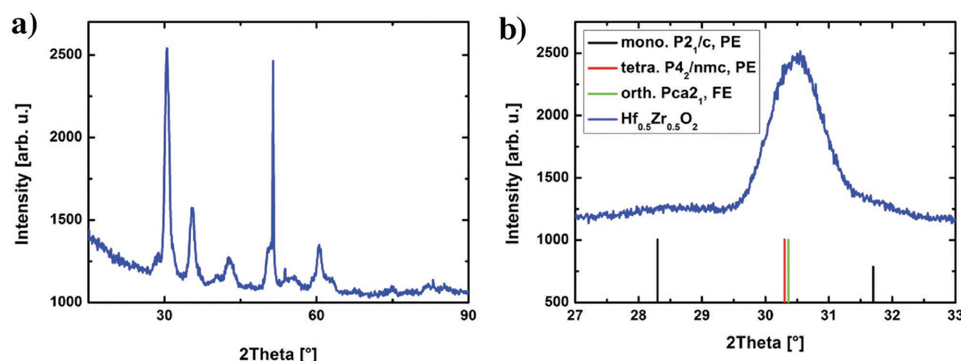

Figure 1. a) Grazing incidence X-ray diffraction results for a 10 nm thick polycrystalline $Hf_{0.5}Zr_{0.5}O_2$ thin film capacitor and b) magnification of peak at 30.5° including reference patterns. The abbreviations refer to the observed polarization behavior: PE: paraelectric, FE: ferroelectric.

caused by an inhomogeneous charge distribution within the sample.[15] These charges can lead to multiple peaks in the current–voltage (*I*–*V*) characteristics, which merge during cycling. With further cycling, a reduction of ferroelectric response (fatigue) is observed.[16] In many cases, dielectric breakdown is then the final limiting factor in the device lifetime. An additional detrimental effect is the shift of the polarization–voltage (*P*–*V*) hysteresis along the voltage axis after a capacitor is exposed to elevated temperatures.[17] This so-called imprint effect might cause a readout failure in memory devices due to a drastically reduced ferroelectric response. All three effects have been thought to relate to oxygen vacancy diffusion,[17] but also electronic contributions[18] and effects of phase change have been discussed.[19,20] However, some of the evidence is indirect and remains to be clarified.

In this study, we analyze the relaxation processes within $Hf_{0.5}Zr_{0.5}O_2$ films in a thickness range of 10–30 nm and compare them to hafnia films containing other dopants and to PZT films. These hafnia thicknesses provide sufficient ferroelectric responses with negligible leakage currents. We analyze the structural and electrical properties of the hafnia–zirconia films and present a field dependence of its fatigue and wake-up, which provides further evidence for the contribution of charges to these effects. Using impedance spectroscopy at various temperatures, we show that defect hopping in a Maxwell–Wagner relaxation process occurs. This hints that at least two distinct layers with different conductivities are present in the film. Consequently, piling up of electrons at low frequency can be expected. Charges in the film are hopping between defect sites. With thermally stimulated depolarization currents (TSDC), we prove the presence of singly and doubly charged oxygen vacancies and calculate the quantity of these mobile defects. Vacancies are mostly caused by consumption of oxygen by the electrodes at the interface[21] between the electrode and film as determined by thickness-dependent TSDC measurements. Additionally, we show that electric field cycling generates additional charged mobile oxygen vacancies in the film. During fatigue, these vacancies act as trapping centers that lead to domain pinning and a reduction of the ferroelectric response. The trapping of electrons at oxygen vacancy sites is therefore one very likely cause for the cycling instability observed in ferroelectric hafnia.

2. Results and Discussion

To analyze the structure of a standard capacitor using a 10 nm thick $Hf_{0.5}Zr_{0.5}O_2$ ferroelectric layer, a grazing incidence X-ray diffraction (GIXRD) measurement was conducted. The resulting diffractogram in **Figure 1**a shows clear peaks, which hints at high crystallinity of the film. A comparison of the peaks between 27° and 33° with the reference spectra in Figure 1b reveals a high fraction of the orthorhombic phase with a minor fraction of the monoclinic phase portion.

High-angle annular dark-field (HAADF) scanning transmission electron microscopy (STEM) reveals additional details, as seen in **Figure 2**a. The films are polycrystalline and contain different polymorphs that are distinguishable by their symmetry and lattice spacing. These changes in structure can be highlighted by fitting the positions of the atom columns and mapping distances to neighboring columns, as shown in Figure 2b.

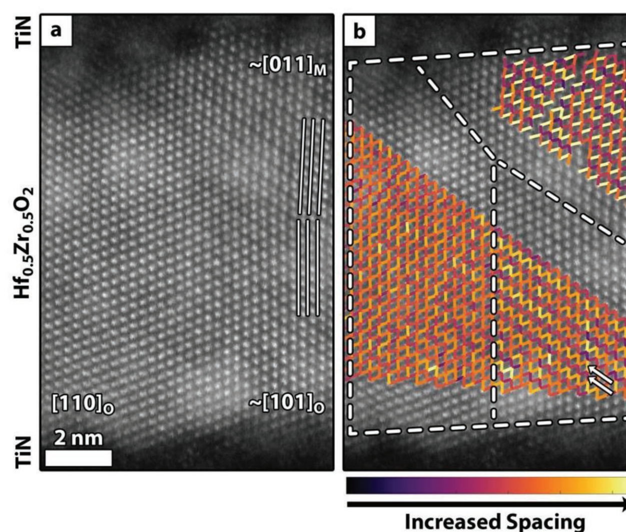

Figure 2. a) HAADF STEM cross section of a 10 nm thick polycrystalline $Hf_{0.5}Zr_{0.5}O_2$ thin film capacitor exhibiting monoclinic and orthorhombic phases, where the {111} (white lines) rotate slightly between the orthorhombic and monoclinic phases. b) Lattice spacing measurements (colored lines) reveal additional subtle changes in the orthorhombic region across a 90° domain wall in the orthorhombic phase.

Provided by Sächsische Landesbibliothek - Staats- und Universitätsbibliothek Dresden

Final edited form was published in "Advanced electronic materials". 2018, 4(3), Art.-Nr. 1700547. ISSN 2199-160X.
https://doi.org/10.1002/aelm.201700547

In Figure 2a, an orthorhombic phase region viewed down the $[110]_o$ zone axis spans the thickness of the film, and forms a 90° domain wall with a neighboring orthorhombic region that is aligned to the$[101]_o$ zone axis (see region boundaries and changes in lattice spacing in Figure 2b). In Figure 2b, arrows lie parallel to $(020)_o$ planes which change to $(002)_o$ planes across the domain boundary. This rotation in the structure results in a change in plane spacing which is visible in the lattice spacing measurements. Both orthorhombic portions also border a monoclinic region that is aligned to the$[011]_m$ zone axis. This monoclinic region has distinct symmetry and spacing compared to the other regions. The {111}-type planes slightly misalign between the orthorhombic and monoclinic phase regions, as indicated by the lines in Figure 2a. The presence of coherent monoclinic/orthorhombic interphase boundaries and 90° orthorhombic domains in $Hf_{0.5}Zr_{0.5}O_2$ is consistent with findings of microstructure in Gd-doped hafnia thin films,[22] which suggests they possess similar microstructure features.[11,20,22] HAADF STEM additionally reveals that the ferroelectric/electrode interface is smoother for the bottom interface than for the top interface, which is consistent with findings for Gd-doped hafnia.[20]

During the ALD deposition process, oxygen from the hafnia film likely reacts with the TiN electrode to form an interfacial TiO_xN region.[21] This causes an asymmetry in the stack with a higher concentration of defects at the top than at the bottom interface.[17] Annealing at higher temperatures initiates the generation of oxygen vacancies due to diffusion of oxygen into the TiN electrode. In parallel, these vacancies are redistributed within the whole HfO_2 layer, which is consistent with a reduced wake-up behavior of samples annealed at higher annealing temperatures.[23] Inhomogeneously distributed oxygen vacancies either near the electrode interface or at phase/domain boundaries, as depicted in Figure 2, are also suspected to be connected to the internal bias field within the sample, which decreases during electric field cycling and causes the wake-up phenomenon.[15]

To further probe this hypothesis of charge-related effects during field cycling, a 15 nm thick $Hf_{0.5}Zr_{0.5}O_2$ layer in a metal–ferroelectric–metal (MFM) capacitor stack was cycled with trapezoidal pulses with 10 µs for each voltage ramp time and plateau time, which yields a cycling frequency of 16.7 kHz. Different electric fields ranging from 2 to 3.3 MV cm^{-1} (see **Figure 3**) were used. In between cycling, polarization–voltage curves were measured using trapezoidal pulses with the same electric field and frequency as used for the cycling pulses. An increase in the memory window $2P_r = (|P_r^- - P_r^+|)$ is evident for voltages lower than 4.5 V which equals electric fields lower than 3 MV cm^{-1}. With increasing field strength, the number of cycles needed to reach the maximum polarization is strongly reduced. This is not caused by a leakage current contribution, because the polarization–voltage curves show no sign of leakage (see Figure 3). Starschich et al. have previously shown that similar samples can be woken up with just a single pulse, attributing their result to oxygen vacancy diffusion.[24] A similar mechanism could explain the absence of wake-up for fields higher than 3 MV cm^{-1}.

The fatigue behavior of these films is a second phenomenon that is strongly influenced by the strength of the applied electric field. The loss of switchable polarization during cycling is strongly reduced with the increasing electric field. This likewise could implicate charge carriers in the film as a reason for the fatigue behavior. Fengler at al.[17] suggested that these charges are most likely pinning domain walls at their seeds (seed inhibition), and that the interfacial layer between ferroelectric and electrode plays a crucial role for this effect.

To further characterize the structure of the pristine 15 nm thick film, impedance spectroscopy measurements at room temperature were performed using an AC signal of 75 mV, an average of 30 measurements, and frequencies ranging from 1 MHz down to 2 Hz (see **Figure 4**). An equivalent circuit was chosen to fit the measurement data, and it consisted of (1) an a resistor in parallel to a capacitor (RC), (2) an element consisting of a constant phase element (CPE) and a resistor in parallel (RCPE), and (3) a simple resistor in series with an RC element (see the inset in Figure 4 and **Table 1**). The RC element represents the bulk properties of the ferroelectric. The second relaxation is represented by the RCPE; thus, an imperfect capacitor has its origin in hopping conduction through the interfacial layer between TiN and the ferroelectric bulk. Such an element is also related to the so-called universal dielectric relaxation, and the Cole–Cole relaxation type, depending on the involved time constants and the considered frequency range.[25] The simple resistor in series with the last RC element represents the imperfect TiN electrode and the contact resistance.[20]

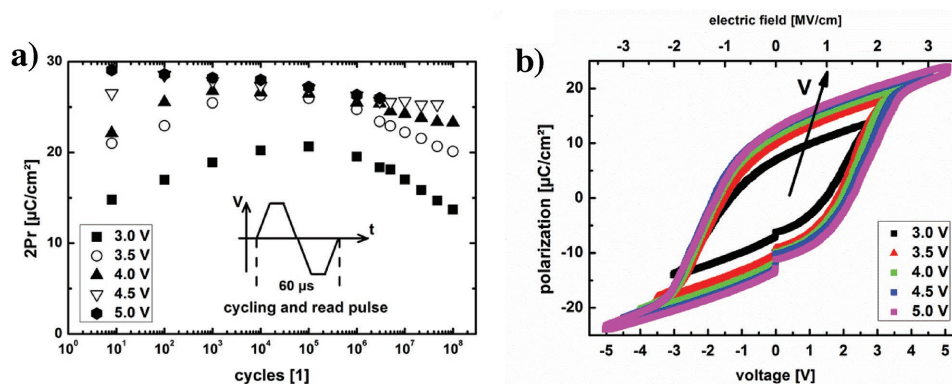

Figure 3. a) Evolution of the memory window of a 15 nm thick $Hf_{0.5}Zr_{0.5}O_2$ film with field cycling. The cycling and measurement was performed with different voltages ranging from 3 to 5 V. b) Polarization-voltage curves after the maximum number of cycles as shown in panel (a).

Provided by Sächsische Landesbibliothek - Staats- und Universitätsbibliothek Dresden

Final edited form was published in "Advanced electronic materials". 2018, 4(3), Art.-Nr. 1700547. ISSN 2199-160X.
https://doi.org/10.1002/aelm.201700547

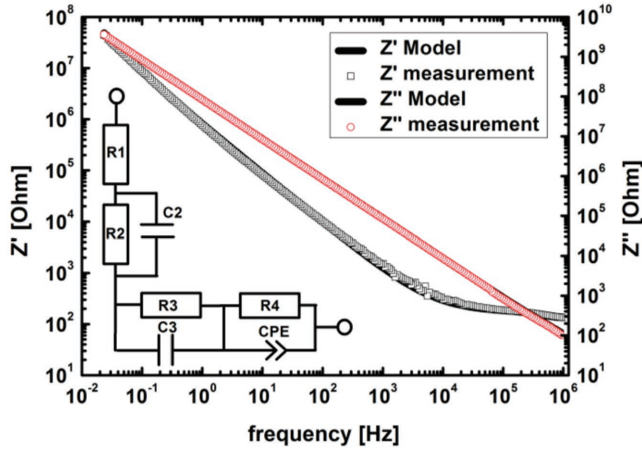

Figure 4. Logarithmic Bode plots generated from the impedance spectroscopy measurements of a 15 nm thick TiN–$Hf_{0.5}Zr_{0.5}O_2$–TiN capacitor.

Similar results to Grimley et al. were achieved.[20] The value close to 1 for the constant phase parameter n (see Table 1) indicates quite homogeneous properties of this layer.[26] The presence of the RCPE relaxation reveals an additional component in the film with different properties compared to the bulk of the material. In literature, where other material systems and thicker layers are investigated, this is often interpreted as the difference between grains and grain boundaries.[27] However, our very thin hafnia thin films consist of mainly columnar grains[22] with a high fraction of oriented grain boundaries[17] strongly decreasing the grain boundary contribution. The significantly more likely possibility is therefore the presence of an interfacial layer as was previously proposed in.[20] This layer could likely contain an increased number of oxygen vacancies compared to the bulk of the material.[17]

Impedance spectroscopy measurements were conducted at elevated temperatures ranging from 275 to 400 °C. To reduce leakage current contributions within the frequency spectrum, 30 nm thick films were utilized. The real and the imaginary components of the dielectric constant, ε' and ε'', were calculated using the relation

$$\varepsilon^* = \varepsilon' - j\varepsilon'' = \frac{1}{j\omega\, C_0\, Z^*} \tag{1}$$

where C_0 denotes the geometric capacitance of the cell (which is the capacitance the cell would have if the dielectric was replaced by vacuum), Z^* the complex impedance, ω the angular frequency, and ε^* the complex permittivity. The real and the imaginary parts of the impedance were plotted as a function of the temperature (see **Figure 5**). At low temperatures, both components are nearly constant. This behavior is well described in literature as nearly constant loss behavior caused by localized motions of dipoles in a double well potential.[28] However, the dielectric constant depends increasingly on the frequency as temperature increases. This is quite likely caused by the universal dielectric response or a Maxwell–Wagner relaxation. As shown by impedance spectroscopy, two components with different conductivities exist within the film. This can cause a piling-up of charge carriers in the low-conductive layer which causes the additional polarization for low frequencies,[27] similar to a Maxwell–Wagner relaxation.

Table 1. Parameters used to fit the impedance spectrum in Figure 4.

Physical interpretation	Abbreviation and unit		Value
Contact resistance	$R1$ [Ω]		1.24×10^{2}
Electrodes	$R2$ [Ω]		4.90
	$C2$ [F]		6.30×10^{-9}
Ferroelectric	$R3$ [Ω]		9.00×10^{13}
	$C3$ [F]		2.10×10^{-9}
Interfacial layer	$R4$ [Ω]		1.00×10^{10}
	CPE (j^n)[Ω]	n	9.58×10^{-1}
		T	1.40×10^{-8}

The impedance loss at low temperatures shows the expected constant enhancement with decreasing frequency caused by the RC component (see **Figure 6**a). At temperatures above 300 °C, however, an additional hump is visible in the analyzed frequency range. This hump is likely connected to the observed Maxwell–Wagner-type relaxation or universal dielectric response and the connected space charges, with the modification that one of the capacitors is a CPE. This contribution shifts to higher frequencies with increasing temperature, which shows that the electrical response is thermally activated. However, the signal of this relaxation strongly overlaps with the constant enhancement of the RC component such that no clear peak can be identified.

For this reason, the complex modulus M^* was analyzed next. The complex modulus $M^*$is defined as

$$M^* = M' + jM'' = j\omega\, C_0 Z^* = \frac{1}{\varepsilon^*} \tag{2}$$

where M' and M'' are the real and imaginary parts of the modulus, respectively.

The modulus approach emphasizes relaxations with small capacitance values.[29] Those contributions can then be more easily analyzed since overlapping relaxations with high capacitance values like bulk responses are suppressed. Peaks in the spectrum of the imaginary part of the modulus (loss) characterize the relaxation frequency of the observed relaxation. The resulting spectra are shown in Figure 6b. No peak can be seen in the investigated frequency regime at room temperature, but starting at 300 °C a single modulus peak can be observed which shifts toward higher frequencies with increasing temperature.

To enable deeper analysis, the peaks are normalized by their maximum value and their peak frequency. The resulting so-called master modulus plot shows that the observed relaxation does not change its distribution with increasing temperature (see Figure 6c). Thus, only one relaxation process with a single activation energy exists within the studied frequency and temperature regime. Furthermore, the peak is broader than expected for a Debye relaxation driven by a simple RC relaxation, where a value of 1.14 decades for the full width at half maximum of the peak would be expected. It is therefore quite likely that a defect relaxation is causal for this observed peak, and that it is related to the CPE involving charge hopping.

The resonance frequency of the modulus loss peak against temperature shows a clear Arrhenius dependence. The activation

Provided by Sächsische Landesbibliothek - Staats- und Universitätsbibliothek Dresden

Final edited form was published in "Advanced electronic materials". 2018, 4(3), Art.-Nr. 1700547. ISSN 2199-160X.
https://doi.org/10.1002/aelm.201700547

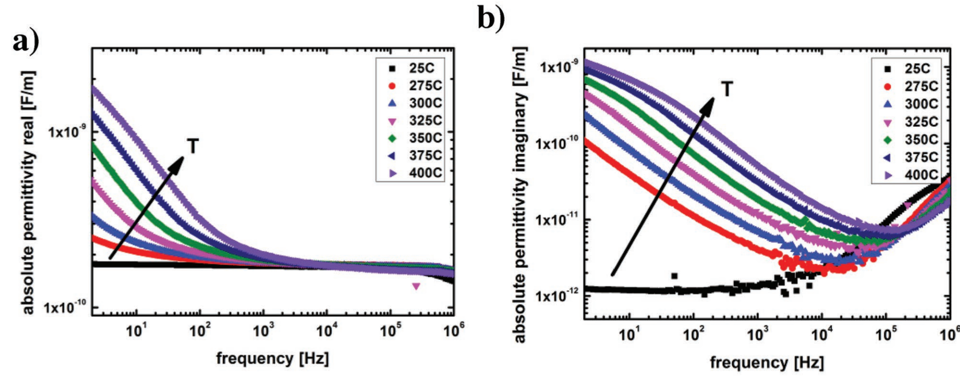

Figure 5. a) Real and b) imaginary parts of the complex permittivity taken from the impedance spectroscopy measurement at different temperatures in the range between 25 and 400 °C.

energy was determined as 1.37 ± 0.01 eV (see Figure 6d). This can be the characteristic for different processes within the hafnia. Defect processes with similar activation energies in hafnia include the hopping of oxygen vacancies,[30] electron hopping between singly negatively charged oxygen vacancies and the neutral state,[31] and between the doubly positively charged oxygen vacancies and the neutral state.[31] In PZT, the resonance frequency of the domain wall motion has been observed for high frequencies up to the high megahertz range.[32] Similar frequencies can be expected for hafnia films. However, domain wall contributions as cause for the observed modulus peak cannot easily be ruled out.

To further examine the possible connection between the relaxation in the modulus spectrum and oxygen vacancies, hafnia films with different dopants (3.5 cat% Gd, 1.5 cat% Al, and 2.5 cat% Si), pure HfO_2, pure ZrO_2, and $Hf_{0.5}Zr_{0.5}O_2$ were tested. Samples were chosen in a similar thickness range of about 30 nm with sufficient ferroelectric properties and high bulk resistances to allow analysis of the RCPE relaxation. Additionally, three 100 nm thick $Pb(Zr_{0.3}Ti_{0.7})O_3$ films were analyzed that were undoped, doped with 2% neodymium, or doped with 2% iron (see **Figure 7** and **Table 2**). For the PZT, a decrease of oxygen vacancy concentration was expected with the transition from Fe doping to undoped to Nd doping of the PZT

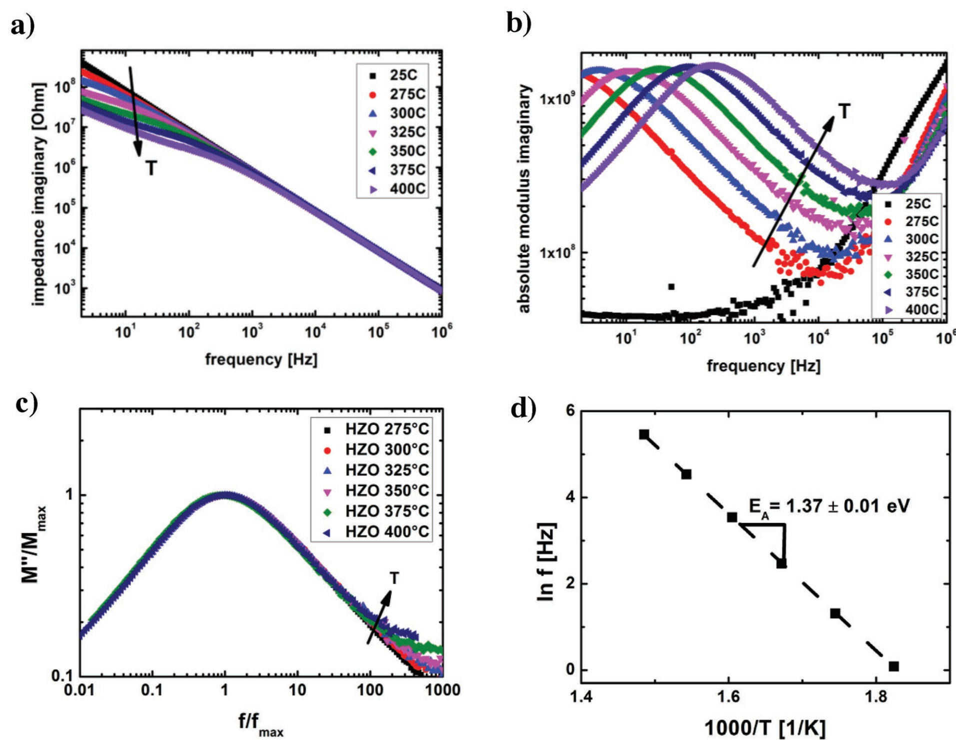

Figure 6. Imaginary part of a) the impedance and b) the modulus at various temperatures between 25 and 400 °C. c) Master modulus plot and d) Arrhenius plot of the shift of the modulus peak.

Provided by Sächsische Landesbibliothek - Staats- und Universitätsbibliothek Dresden

Final edited form was published in "Advanced electronic materials". 2018, 4(3), Art.-Nr. 1700547. ISSN 2199-160X.
https://doi.org/10.1002/aelm.201700547

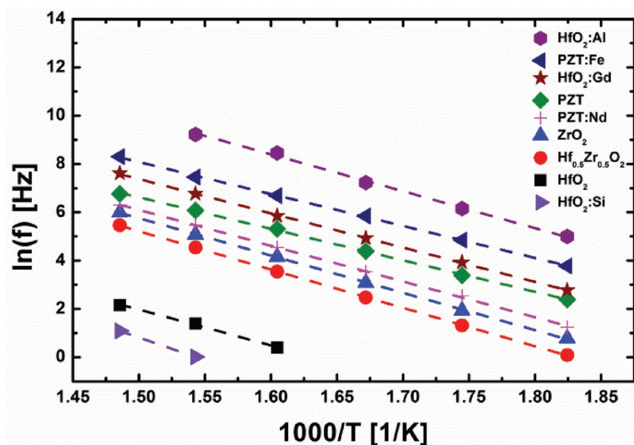

Figure 7. Arrhenius plots of the shift of the modulus peak frequency for various samples.

film due to the different dopant valance and site occupancy in the PZT crystal. While Nd^{3+} occupies the A-site and reduces the amount of oxygen vacancies, Fe^{3+} occupies the B-site and increases the oxygen vacancy content of PZT film.[20,33,34] For hafnia films, an increase in oxygen vacancy concentration is expected with decreasing valence. A shift of the modulus peak toward lower frequencies with increasing valence of the dopant was observed for all material systems. This strongly suggests a relation between the charge hopping process observed in the modulus spectrum and the oxygen vacancy concentration in the film. Since the presence of a loss peak is also observed for nonpolar HfO_2 (see Figure 7), domain wall contributions can be neglected. Point defects such as electrons at oxygen vacancy sites are most likely the cause.

To identify the responsible charge carriers for the relaxation in the impedance spectrum, thermally stimulated depolarization current measurements were conducted on a 10 nm thick $Hf_{0.5}Zr_{0.5}O_2$ film. As a first step, the samples were polarized for 800 s at 380 °C with an applied voltage ranging from 0.5 to 1.5 V. This step is followed by rapid cooling while still applying the same electric field to freeze possible diffused charges in their local and energetic positions. Additionally, poling with 3.0 V was conducted at 25 °C. By slowly heating up the sample with 0.2 K s^{-1}, the depolarization current was measured

Table 2. Extracted activation energies with standard error for the linear fits of Figure 7.

	Dopant valence	E_A [eV]	Standard error
HfO_2:Al	3	1.32	±0.04
HfO_2:Gd	3	1.22	±0.01
ZrO_2	4	1.33	±0.01
$H_{0.5}Zr_{0.5}O_2$	4	1.37	±0.01
HfO_2	4	1.28	±0.07
HfO_2:Si	4	(1.62)	
PZT:Fe	3	1.14	±0.01
PZT		1.12	±0.01
PZT:Nd	3	1.28	±0.01

(see **Figure 8**). No peaks were seen for poling at room temperature. In contrast to room temperature, two overlapping peaks were observed with maxima around 220 and 350 °C after poling at 380 °C.

To separate the peaks, the thermal cleaning method was used.[35] The peak at 350 °C was measured solely by poling the sample at 320 °C and relaxing the charges with lower activation energy by holding the temperature at 250 °C for 800 s without an applied field before cooling down to room temperature (see **Figure 9**a). The lower-temperature peak was separated by reducing the poling temperature to 200 °C (see Figure 9b), which does not allow charges with high diffusion activation energies to move significantly. By using the slopes of the peaks (initial rise method),[36] activation energies were extracted ranging from 0.52 to 0.62 eV for the low-temperature peak (see Figure 9c) and ranging from 1.04 to 1.24 eV for the high-temperature peak (see Figure 9d) depending on the applied poling field strength. These values are in agreement with reported calculated values for the diffusion of singly (1.2 eV)[30] and doubly charged oxygen vacancies (0.7 eV).[30,37] Additionally, it can be seen that no significant diffusion of these charged vacancies occurs at temperatures below 100 °C and the applied voltages up to 1.5 V (see Figure 8). At room temperature with an applied voltage of 3 V (see Figure 8), which is the lower limit of the switching field used for endurance tests, no oxygen vacancy diffusion was detected. It therefore seems unlikely that oxygen vacancy diffusion contributes in a major way to wake-up phenomenon (see Figure 3) or the imprint effect,[17] which both occur at lower temperatures.

By using the activation energy E_A, the heating ramp rate q, and the temperature T_p at which the maximum current for the diffusion process was observed, an equivalent frequency can be calculated at which the hopping process under an AC field should occur[38]

$$f_{AC} = \frac{\omega}{2\pi} = \frac{1}{2\pi}\frac{qEA}{k_B T_P^2} \quad (3)$$

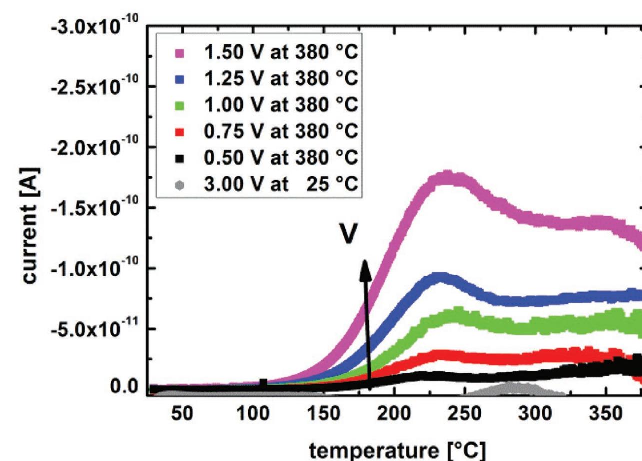

Figure 8. Thermally stimulated depolarization current measurement of 10 nm thick TiN–$Hf_{0.5}Zr_{0.5}O_2$–TiN capacitors using a ramp rate of 0.2 K s^{-1} after poling with voltages between 0.5 and 1.5 V in steps of 0.25 V for 800 s at 380 °C and with 3.0 V for 800 s at 25 °C. The different colors indicate the different polling voltages.

Provided by Sächsische Landesbibliothek - Staats- und Universitätsbibliothek Dresden

Final edited form was published in "Advanced electronic materials". 2018, 4(3), Art.-Nr. 1700547. ISSN 2199-160X.
https://doi.org/10.1002/aelm.201700547

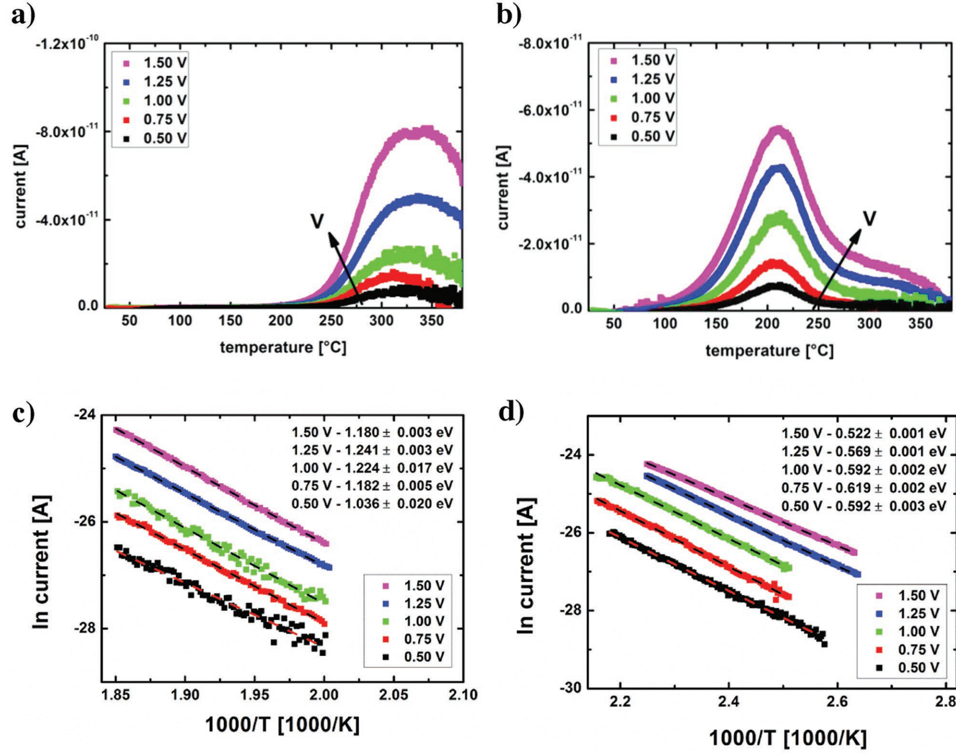

Figure 9. Thermally stimulated depolarization current measurement of 10 nm thick TiN–$Hf_{0.5}Zr_{0.5}O_2$–TiN capacitors using a ramp rate of 0.2 K s^{-1}: a) after poling with voltages between 0.5 and 1.5 V in steps of 0.25 V for 800 s at 320 °C and thermal cleaning at 250 °C for 800 s, and b) after poling with voltages between 0.5 and 1.5 V in steps of 0.25 V for 800 s at 200 °C and Arrhenius plots of the initial slope of the TSDC peaks with extracted activation energies using thermal rise method.

For both TSDC peaks, the corresponding hopping frequency of oxygen vacancies in the modulus spectrum would be therefore expected in the low millihertz range. However, the frequency range in impedance spectroscopy is from 2 Hz to 1 MHz. Therefore, the observed modulus peaks in impedance spectroscopy are more likely caused by electron hopping between defect states than by ion hopping itself.

The amount of diffused charges Q_{TSDC} was calculated by integration of the current peaks. It was not possible to measure the complete high-temperature peak within the observed temperature regime, and the low-temperature peak showed small distortions above 260 °C (possibly due to some residual doubly charged oxygen vacancies). For these reasons, the depolarization current peaks were assumed to be symmetric, and the charge was calculated by doubling the integral of the peak area from the low-temperature side of the peak maximum for all voltages. The earlier calculated activation energies and low equivalent frequencies strongly point to the existence and the diffusion of charged oxygen vacancies as the origin of the two TSDC peaks. The voltage dependence of the amount of diffused charges Q_{TSDC} should therefore follow[39]

$$Q_{TSDC} = Q_0 \sinh \frac{qaV_b}{2k_BT_b} \tag{4}$$

where Q_{TSDC} is identical to the integrated charges of the TSDC peak, Q_0 is the total amount of mobile charged ions present, q is the ionic charge, a is the hopping distance, V_b is the applied bias voltage, k_B is the Boltzmann constant, and T_b is the temperature at which the TSDC peak was observed. By fitting the measured data to the simplified function

$$Q_{TSDC} = Q_0 \sinh B \tag{5}$$

the quantity of mobile charge carriers per volume was extracted for both peaks (see **Figure 10**a, b and **Table 3**). Since the observed dependence shows a nonlinear sinh dependence dielectric polarization as possible cause of the depolarization currents can be excluded.[39]

The most likely positions of the vacancies within the orthorhombic hafnia lattice are the three-coordinate O-sites (O^3).[37,40,41] The amount of oxygen vacancies Q_V was calculated for the absolute number of O^3 sites within the film by

$$Q_V = \frac{Q_0}{AdN_{O^3}a} \tag{6}$$

where A denotes the capacitor area, Q_0 the amount of mobile charges, d the film thickness, N_{O^3} the number of three-coordinate O-sites per centimeter of 2.956×10^{22} cm^{-3}. within the orthorhombic hafnia crystal structure, and a the valency of the ion.

The amount of singly and doubly charged oxygen vacancies was calculated as 0.26% and 0.10% of the O^3 sites within the film. This amount is surprisingly low, but is similar in order of magnitude to calculated values of defects in Sr-doped Hf[43]

Provided by Sächsische Landesbibliothek - Staats- und Universitätsbibliothek Dresden

Final edited form was published in "Advanced electronic materials". 2018, 4(3), Art.-Nr. 1700547. ISSN 2199-160X.
https://doi.org/10.1002/aelm.201700547

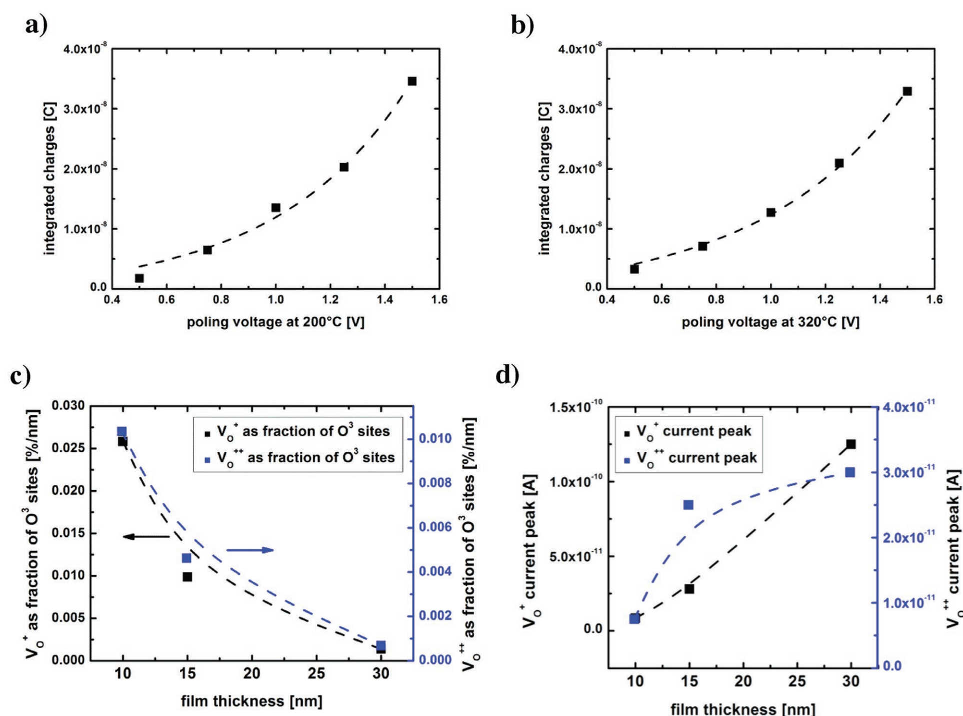

Figure 10. Charges extracted from the depolarization current measurements of 10 nm thick TiN–$Hf_{0.5}Zr_{0.5}O_2$–TiN capacitors using a ramp rate of 0.2 K s^{-1}: a) after poling with voltages between 0.5 and 1.5 V in steps of 0.25 V for 800 s at 320 °C and thermal cleaning at 250 °C for 800 s; b) after poling with voltages between 0.5 and 1.5 V in steps of 0.25 V for 800 s at 200 °C; c) extracted number of singly and doubly positively charged oxygen vacancies of 10, 15, and 30 nm thick TiN–$Hf_{0.5}Zr_{0.5}O_2$–TiN capacitors; and d) extracted maximum current in the thermally stimulated depolarization current measurement after thermal cleaning and poling with 0.5 V of the corresponding charged oxygen vacancies V_O^+ at about 250 °C and V_O^{++} at about 320 °C

and might be reasonable if, as suggested by Fengler et al.,[17] seed inhibition is dominating imprint and possibly the wake-up mechanism. Additionally, it must be noted that only mobile charged defects can be measured with the TSDC method, whereas neutral and immobile defects remain undetected. Neutral vacancies are known to also cause domain wall pinning in PZT films.[42] Therefore, the real total amount of defects in the film might be higher. For seed inhibition as a working mechanism, the oxygen vacancies would have to be mainly present close to the electrode/ferroelectric interface as trapping sites. To test this hypothesis, the dependence of the oxygen vacancy concentration on the film thickness was analyzed (see Figure 10c).

A clear reduction of the charged oxygen vacancies with increasing thickness can be observed. This shows, that the observed TSDC peak is not induced by a simple electrode polarization, which would be thickness independent. The thickness dependence of the maximum current at the TSDC peak (see Figure 10d) also proves that electrons are not the cause for the TSDC peaks. The observed peak height increases with enhanced film thickness, which is characteristic for ions instead of staying constant as it would be the case for electrons. On the other hand, it might hint at a higher concentration of these defects at the interface as suggested in ref. [43] However, a higher portion of monoclinic phase for higher thicknesses[44] could cause another defect composition and defect mobility within the film, which might influence this result. In addition, it is possible that even though the oxygen vacancies are caused by the reaction of the electrode with the film, they might diffuse through the film during the high-temperature processing step. A similar thickness dependence would be the result. Hence, the exact position of the defects before poling cannot be unambiguously deduced.

To analyze the influence of electric field cycling on the defect concentration, precycled 30 nm thick samples were measured. The capacitor structures were cycled with 10^6 trapezoidal pulses of 2.7 MV cm^{-1} with 10 µs for each voltage ramp time and plateau time, which corresponds to the chosen

Table 3. Parameters used to fit the dependency of the integrated charges on the poling voltage, as shown in Figures 10 and 11, and the standard error.

	Q_0	Standard error	B	Standard error
220 °C peak				
10 nm	2.94×10^{-9}	0.75×10^{-9}	2.11	0.18
15 nm	2.96×10^{-9}	0.60×10^{-9}	1.77	0.14
30 nm	0.75×10^{-9}	0.56×10^{-9}	2.02	0.05
30 nm cycled	1.66×10^{-9}	0.22×10^{-9}	1.65	0.09
350 °C peak				
10 nm	3.67×10^{-9}	0.42×10^{-9}	1.93	0.08
15 nm	3.15×10^{-9}	0.51×10^{-9}	2.21	0.11
30 nm	2.09×10^{-9}	0.39×10^{-9}	2.93	0.13
30 nm cycled	7.08×10^{-9}	0.55×10^{-9}	2.19	0.06

Provided by Sächsische Landesbibliothek - Staats- und Universitätsbibliothek Dresden

Final edited form was published in "Advanced electronic materials". 2018, 4(3), Art.-Nr. 1700547. ISSN 2199-160X.
https://doi.org/10.1002/aelm.201700547

frequency of 16.7 kHz (see **Figure 11**a). The larger film thickness and lower electric fields were necessary to reduce leakage currents and to decrease the risk of dielectric breakdown during TSDC measurements.

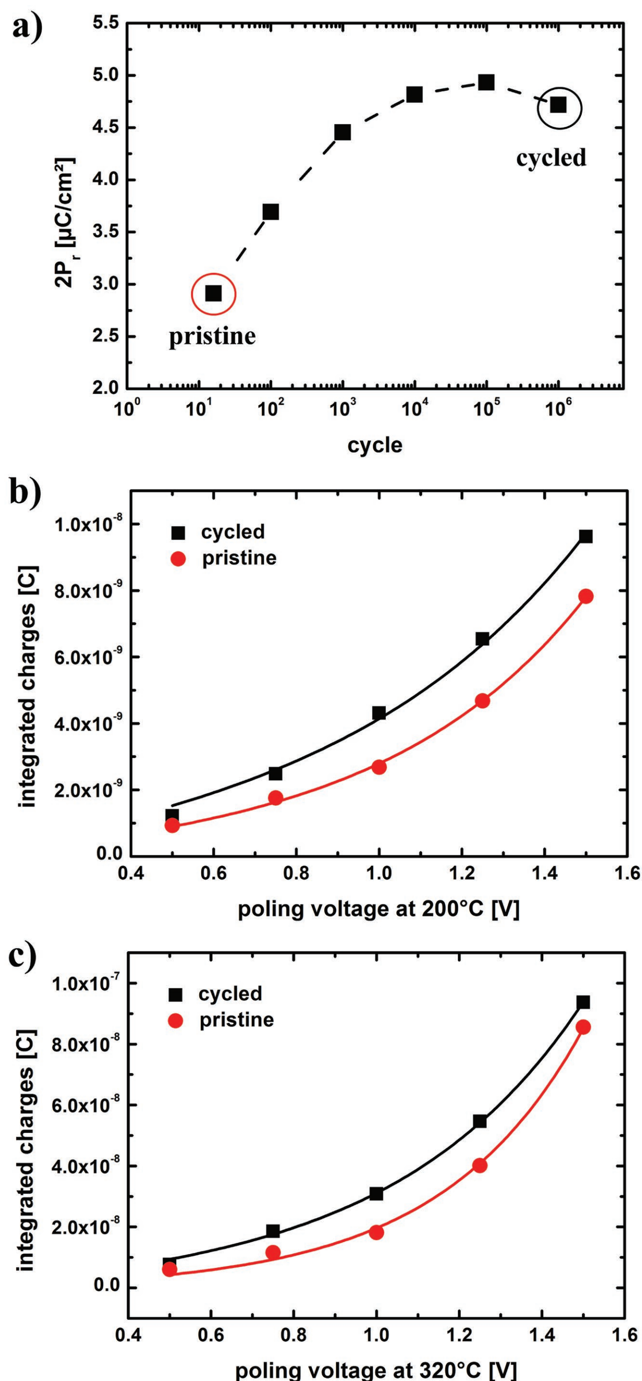

Figure 11. Charges extracted from thermal depolarization current measurements on 30 nm thick TiN–$Hf_{0.5}Zr_{0.5}O_2$–TiN capacitors using a ramp rate of 0.2 K s^{-1} before and after cycling as shown in a) with 2.7 MV cm^{-1} at 16.7 kHz.: b) after poling with voltages between 0.5 and 1.5 V in steps of 0.25 V for 800 s at 200 °C and c) after poling with voltages between 0.5 and 1.5 V in steps of 0.25 V for 800 s at 320 °C and subsequent thermal cleaning at 250 °C for 800 s.

Using the same TSDC procedure as described before, the concentrations of singly and doubly charged oxygen vacancies were calculated and compared with those of uncycled capacitors of the same film (see Figure 11b,c and Table 3). The doubly positively charged oxygen vacancy concentration increased from 0.009% in the initial state to 0.019% after wake-up by electric field cycling. A similar trend can be observed for the singly positively charged oxygen vacancy concentration which increases from 0.049% to 0.166%. The increased number of positively charged oxygen vacancies also increases the chance of electron trapping within the film, which might lead to domain wall pinning.

Overall, it was shown that a combination of impedance spectroscopy in conjunction with TSDC is very useful to characterize the charge movement during field cycling and to distinguish between electron hopping between different defect states and the related diffusion of oxygen vacancies.

3. Conclusion

Ferroelectric $Hf_{0.5}Zr_{0.5}O_2$ films were cycled with different electric fields. During this electric cycling, a strong dependence of wake-up and fatigue on electric field strength was observed, and the influence of internal charges was suspected as cause. Impedance spectroscopy analysis and previous works hint at the presence of an interfacial layer between electrodes and ferroelectric. Modulus spectroscopy measurements at different temperatures reveal that a Maxwell–Wagner relaxation due to space charges most likely occurs in the interfacial layer. The obtained activation energy for the shift of the modulus loss peak of 1.37 eV and its dependence on the valence of the dopant in the hafnia system suggest oxygen vacancies as trapping sites. Thermally stimulated depolarization current measurements were conducted showing two distinct relaxation current peaks. The extracted activation energies for the diffusion of the causal charge carriers were 0.52–0.62 and 1.04–1.24 eV depending on the applied poling field. These values are in good agreement with reported activation energies for diffusion of singly and doubly charged oxygen vacancies of 1.2 and 0.7 eV, respectively. Additionally, it was shown that no diffusion of charged oxygen vacancies was observed under the measurement conditions at room temperature. Diffusion of oxygen vacancies as the cause for the imprint phenomenon is therefore unlikely. For the wake-up effect, it cannot fully be excluded since the diffusion of charged oxygen vacancies under an applied field strength as used in ferroelectric switching is possible in general and well established in resistive switching applications.[45,46] However, diffusion of charged oxygen vacancies as sole cause is unlikely since the applied field during cycling is rather low and alternating. Moreover, in contrast to resistive switching, we do not deal with rather high density of localized current leading to additional Joule heating that can significantly enhance diffusion processes. Using the poling field dependence, the concentration of singly and doubly charged oxygen vacancies was calculated to be in the subpercent range of the O^3 sites. Therefore, most of the present oxygen defects might be in a neutral state or immobile under the investigated fields and temperatures.

Provided by Sächsische Landesbibliothek - Staats- und Universitätsbibliothek Dresden

Final edited form was published in "Advanced electronic materials". 2018, 4(3), Art.-Nr. 1700547. ISSN 2199-160X.
https://doi.org/10.1002/aelm.201700547

Films of different thickness were measured, and a reduction of charged defect concentration with increasing thickness was found. This hints at a higher defect concentration at the interface between film and electrode. Finally, the influence of electric field cycling was analyzed, and a strong increase of singly and doubly charged oxygen vacancies was found after field cycling. These can cause an increased trapping of electrons in the ferroelectric and pinning of domain walls, which seems to be the cause of the performance instabilities of hafnia. Possible solutions for future devices might be a reduction of oxygen vacancies at the interface by, e.g., oxide electrodes. Alternatively, a sequential detrapping approach by a pulse with high electric field, or heating the sample to allow charge diffusion, might lead to future performance improvements.

4. Experimental Section

Planar MFM capacitor stacks were prepared on silicon substrates. 100 nm thick 2% Fe-doped 30/70 PZT samples were fabricated by chemical solution deposition processing of a butanol-based precursor solution which was synthesized according to a route published elsewhere.[45] Iron acetyl acetonate was used as a source for the iron doping and added to the other educts for solution synthesis. The 0.3 mol L^{-1} coating solution was applied to the platinized silicon substrate at room temperature by spin-coating at 3000 rpm for 30 s. Subsequently, the as-deposited layer was pyrolyzed at 350 °C for 2.5 min on a hot plate. After one repetition of this sequence the two-layer stack was crystallized at 700 °C by rapid thermal annealing for 5 min, which caused crystallization and a preferred (111) orientation of the film (GIXRD). Pt top electrodes were deposited by sputtering and lift-off patterning.[17]

Then, 10–30 nm thick $Hf_{0.5}Zr_{0.5}O_2$ films were grown in an Oxford Instruments OpAL ALD tool using Hf- and Zr-metalorganic precursors similar to the ones used in previous publications.[47] Under the given ALD conditions, HZO films with an Hf:Zr ratio of 0.5:0.5 were deposited applying an HfO_2:ZrO_2 ALD cycle ratio of 1:1 and using H_2O as the oxygen source. As reported before, TiN electrodes were deposited before and after dielectric deposition. In order to stabilize the orthorhombic phase, the samples were annealed slightly above the $Hf_{0.5}Zr_{0.5}O_2$ crystallization temperature of 400 °C after the deposition of the top electrode in an AST rapid thermal processing tool under N_2 atmosphere.

Then, 30 nm thick HfO_2 doped with Si was deposited in an ALD reactor using tetrakis[ethylmethylamino]hafnium (TEMAHf, $Hf(N(CH_3)(C_2H_5))_4$), *N*,*N*,*N*′,*N*′-tetraethylsilanediamine (SAM.24, $H_2Si[N(C_2H_5)_2]_2$), and H_2O as the oxygen source similar to ref. [48]. TiN electrodes were deposited before and after dielectric deposition. The stack was annealed in an AST rapid thermal processing tool under N_2 atmosphere at 550 °C after the deposition of the top electrode for 10 min to crystallize the film.

30 nm thick HfO_2 doped with 3.5 cat% Gd was deposited in an ALD process as described in refs. [6] and .[49] TiN electrodes were deposited before and after deposition. The capacitor stack was annealed at 450 °C for 10 min in an AST rapid thermal processing tool under N_2 atmosphere.

The 30 nm thick HfO_2 doped with Al was deposited with a cycle ratio of 24:1 in an ALD process at 200 °C using TEMAHf, $Hf(N(CH_3)(C_2H_5))_4$) and trimethylaluminum, and water as the oxygen source. The capacitor stack was annealed at 800 °C for 30 s.

The gracing incidence X-ray measurement was conducted using a Bruker D8 Discover X-ray diffraction tool with Cu Kα radiation of 0.154 nm wavelength and a fixed incidence angle of 0.5° for the 2Theta scan.

The STEM lamella was prepared using an FEI Helios Nanolab 600i dual beam. HAADF STEM was performed using a probe aberration-corrected Nion UltraSTEM 100 operated at 100 kV with a probe semiconvergence angle of 31 mrad and a detector inner semiangle of ≈86 mrad. Atom column indexing and lattice analysis were facilitated by Gaussian peak fitting and matrix indexing as described previously.[50]

Electrical characterization was performed on a Cascade Microtech RF Probe Station with an aixACCT TF Analyzer 3000 and a Keithley 4200 Semiconductor Characterization System. TSDC measurements were performed on a Micromanipulator 8065 Probe Station with a Stanford Research Systems PTC 10 Programmable Temperature Controller and an Agilent 4156 B. Impedance and modulus spectroscopy was performed on a Micromanipulator 8065 Probe Station using a Solartron 1260 Impedance/Gain-Phase Analyzer and a 1296A dielectric interface system including a 12961 reference module.

Acknowledgements

E.D.G. and J.M.L. gratefully acknowledge support from the National Science Foundation (DMR-1350273). E.D.G. acknowledges support for this work through a National Science Foundation Graduate Research Fellowship (DGE-1252376). STEM imaging was conducted at the Center for Nanophase Materials Sciences, which is a DOE Office of Science User Facility. The authors thank Tina Sturm and Almut Poehl from Leibniz IFW Dresden, Germany for preparing the STEM lamella, Sergej Starschich, Theodor Schneller, and Ulrich Böttger from the RWTH Aachen for the preparation of the PZT films and M.Sc. Felix Winkler from TU Dresden (IHM) for providing the high-temperature measurement setup. Christoph Adelmann from Imec, Belgium is gratefully acknowledged for the deposition of the TiN/Gd:HfO_2/TiN stacks.

Conflict of Interest

The authors declare no conflict of interest.

Keywords

electron trapping, ferroelectric, hafnium oxide, impedance spectroscopy, oxygen vacancies, thermally stimulated depolarization current

Received: November 6, 2017
Revised: January 3, 2018
Published online: February 1, 2018

[1] J. S. Meena, S. M. Sze, U. Chand, T. Y. Tseng, *Nanoscale Res. Lett.* **2014**, *9*, 526.
[2] Ramtron, *Ramtron Announces 8-Megabit Parallel Nonvolatile F-RAM Memory*, Ramtron International Corporation, Colorado Springs, CO **2009**.
[3] Y. Fujisaki, *IEICE Electron. Exp.* **2012**, *9*, 908.
[4] M. T. Bohr, R. S. Chau, T. Ghani, K. Mistry, *IEEE Spectrum* **2007**, *10*, 23.
[5] T. S. Boescke, J. Mueller, D. Braeuhaus, U. Schroeder, U. Boettger, *Appl. Phys. Lett.* **2011**, *99*, 102903.
[6] S. Mueller, C. Adelmann, A. Singh, S. Van Elshocht, U. Schroeder, T. Mikolajick, *ECS J. Solid State Sci. Technol.* **2012**, *1*, N123.
[7] J. Mueller, T. S. Boscke, S. Mueller, E. Yurchuk, P. Polakowski, J. Paul, D. Martin, T. Schenk, K. Khullar, A. Kersch, W. Weinreich, S. Riedel, K. Seidel, A. Kumar, T. M. Arruda, S. V. Kalinin, T. Schlosser, R Boschke, R. van Bentum, U. Schroeder, T Mikolajick, in *2013 IEEE Int. Electron Devices Meeting (IEDM)*, IEEE, San Francisco CA, USA **2013**, pp. 10.8.1–10.8.4, https://doi.org/10.1109/IEDM.2013.6724605.

Provided by Sächsische Landesbibliothek - Staats- und Universitätsbibliothek Dresden

Final edited form was published in "Advanced electronic materials". 2018, 4(3), Art.-Nr. 1700547. ISSN 2199-160X.
https://doi.org/10.1002/aelm.201700547

[8] T. Schenk, S. Mueller, U. Schroeder, R. Materlik, A. Kersch, M. Popovici, C. Adelmann, S. Van Elshocht, T Mikolajick, in *2013 Proc. of the European Solid-State Device Research Conf. (ESSDERC)*, IEEE, Bucharest, Romania **2013**, p. 260, https://doi.org/10.1109/ESSDERC.2013.6818868.
[9] S. Mueller, J. Mueller, A. Singh, S. Riedel, J. Sundqvist, U. Schroeder, T. Mikolajick, *Adv. Funct. Mater.* **2012**, *22*, 2412.
[10] J. Mueller, U. Schroeder, T. S. Boescke, I. Mueller, U. Boettger, L. Wilde, J. Sundqvist, M. Lemberger, P. Kuecher, T. Mikolajick, L. Frey, *J. Appl. Phys.* **2011**, *110*, 114113.
[11] X. Sang, E. D. Grimley, T. Schenk, U. Schroeder, J. M. LeBeau, *Appl. Phys. Lett.* **2015**, *106*, 162905.
[12] J. Mueller, T. S. Boescke, U. Schroeder, S. Mueller, D. Braeuhaus, U. Boettger, L. Frey, T. Mikolajick, *Nano Lett.* **2012**, *12*, 4318.
[13] M. Pešić, S. Knebel, M. Geyer, S. Schmelzer, U. Boettger, N. Kolomiiets, V. V. Afanas'ev, K. Cho, C. Jung, J. Chang, H. Lim, T. Mikolajick, U. Schroeder, *J. Appl. Phys.* **2016**, *119*, 064101.
[14] International Technology Roadmap for Semiconductors. Process Integration, Devices, and Structures 3. Technical Report, http://www.itrs2.net/itrs-reports.html, **2013**.
[15] T. Schenk, M. Hoffmann, J. Ocker, M. Pešić, T. Mikolajick, U. Schroeder, *ACS Appl. Mater. Interfaces* **2015**, *7*, 20224.
[16] T. Schenk, U. Schroeder, M. Pešić, M. Popovici, Y. V. Pershin, T. Mikolajick, *ACS Appl. Mater. Interfaces* **2014**, *6*, 19744.
[17] F. P. G. Fengler, M. Pešić, S. Starschich, T. Schneller, C. Kuenneth, U. Boettger, H. Mulaosmanovic, T. Schenk, M. H. Park, R. Nigon, P. Muralt, T. Mikolajick, U. Schroeder, *Adv. Electron. Mater.* **2017**, *3*, 1600505, https://doi.org/10.1002/aelm.201600505.
[18] M. Pešić, S. Slesazeck, T. Schenk, U. Schroeder, T. Mikolajick, *Phys. Status Solidi* **2016**, *213*, 270.
[19] M. H. Park, H. J. Kim, Y. J. Kim, Y. H. Lee, T. Moon, K. D. Kim, S. D. Hyun, F. P. G. Fengler, U. Schroeder, C. S. Hwang, *ACS Appl. Mater. Interfaces* **2016**, *8*, 15466.
[20] E. D. Grimley, T. Schenk, X. Sang, M. Pešić, U. Schroeder, T. Mikolajick, J. M. LeBeau, *Adv. Electron. Mater.* **2016**, *2*, 1600173.
[21] W. Weinreich, R. Reiche, M. Lemberger, G. Jegert, J. Müller, L. Wilde, S. Teichert, J. Heitmann, E. Erben, L. Oberbeck, U. Schroeder, A. J. Bauer, H. Ryssel, *Microelectron. Eng.* **2009**, *86*, 1826.
[22] E. D. Grimley, T. Schenk, T. Mikolajick, U. Schroeder, J. M. LeBeau, *Adv. Mater. Interfaces* **2018**, 1701258, https://doi.org/10.1002/admi.201701258.
[23] T. Mittmann, F. P. G. Fengler, C. Richter, M. H. Park, T. Mikolajick, U. Schroeder, *Microelectron. Eng.* **2017**, *178*, 48.
[24] S. Starschich, S. Menzel, U. Boettger, *J. Appl. Phys.* **2017**, *121*, 154102.
[25] J. Y. Fu, *Philos. Mag.* **2014**, *94*, 1788.
[26] Z. Kerner, T. Pajkossy, *Electrochim. Acta* **2000**, *46*, 207.
[27] R. Tang, C. Jiang, W. Qian, J. Jian, X. Zhang, H. Wang, H. Yang, *Sci. Rep.* **2015**, *5*, 13645.
[28] K. S. Gilroy, W. A. Phillips, *Philos. Mag. B* **1981**, *43*, 735.
[29] K. Prabakar, S. K. Narayandass, D. Mangalaraj, *Mater. Sci. Eng. B* **2003**, *98*, 225.
[30] C. Li, Y. Yao, X. Shen, Y. Wang, J. Li, C. Gu, R. Yu, Q. Liu, M. Liu, *Nano Res.* **2015**, *8*, 3571.
[31] K. Xiong, J. Robertson, M. C. Gibson, S. J. Clark, *Appl. Phys. Lett.* **2005**, *87*, 183505.
[32] M. I. Morozov, D. Damjanovic, *J. Appl. Phys.* **2010**, *107*, 034106.
[33] R. A. Eichel, *Phys. Chem. Chem. Phys.* **2011**, *13*, 368.
[34] L. Wu, T. S. Wu, C. C. Wei, H. Liu, *J. Phys. C: Solid State Phys.* **1983**, *16*, 2823.
[35] J. F. Mano, *J. Phys. D: Appl. Phys.* **1998**, *31*, 2898.
[36] W. Liu, C. A. Randall, *J. Am. Ceram. Soc.* **2008**, *91*, 3245.
[37] N. Capron, P. Broqvist, A. Pasquarello, *Appl. Phys. Lett.* **2007**, *91*, 192905.
[38] *Thermally Stimulated Relaxation in Solids* (Ed: P. Braeunlich), Springer, Berlin, Germany **1979**.
[39] T Hino, *IEEE Trans. Electr. Insul.* **1980**, *15*, 301, https://doi.org/10.1109/TEI.1980.298323.
[40] P. Broqvist, A. Pasquarello, *Appl. Phys. Lett.* **2006**, *89*, 262904.
[41] A. S. Foster, F. L. Gejo, A. L. Shluger, R. M. Nieminen, *Phys. Rev. B* **2002**, *65*, 174117.
[42] A. Chandrasekaran, D. Damjanovic, N. Setter, N. Marzari, *Phys. Rev. B* **2013**, *88*, 214116.
[43] M. Pešić, F. P. G. Fengler, L. Larcher, A. Padovani, T. Schenk, E. D. Grimley, X. Sang, J. M. LeBeau, S. Slesazeck, U. Schroeder, T. Mikolajick, *Adv. Funct. Mater.* **2016**, *26*, 4601.
[44] M. Hoffmann, U. Schroeder, T. Schenk, T. Shimizu, H. Funakubo, O. Sakata, D. Pohl, M. Drescher, C. Adelmann, R. Materlik, A. Kersch, T. Mikolajick, *J. Appl. Phys.* **2015**, *118*, 072006.
[45] T. Schneller, H. Kohlstedt, A. Petraru, R. Waser, J. Guo, J. Denlinger, T. Learmonth, P.-A. Glans, K. E. Smith, *J. Sol-Gel Sci. Technol.* **2008**, *48*, 239.
[46] S. Kumar, Z. Wang, X. Huang, N. Kumari, N. Davila, J. P. Strachan, D. Vine, A. L. D. Kilcoyne, Y. Nihi, R. S. Williams, *Appl. Phys. Lett.* **2017**, *110*, 103503.
[47] A. Chernikova, M. Kozodev, A. Markeev, D. Negrov, M. Spiridonov, S. Zarubin, O. Bak, P. Buragohain, H. Lu, E. Suvorova, A. Gruverman, A. Zenkevich, *ACS Appl. Mater. Interfaces* **2016**, *8*, 7232.
[48] C. Richter, T. Schenk, M. H. Park, F. A. Tscharntke, E. D. Grimley, J. M. LeBeau, C. Zhou, C. M. Fancher, J. L. Jones, T. Mikolajick, U. Schroeder, *Adv. Electron. Mater.* **2017**, *3*, 1700131.
[49] C. Adelmann, H. Tielens, D. Dewulf, A. Hardy, D. Pierreux, J. Swerts, E. Rosseel, X. Shi, M. K. Van Bael, J. A. Kittl, S. Van Elshocht, *J. Electrochem. Soc.* **2010**, *157*, G105.
[50] X. Sang, A. A. Oni, J. M. LeBeau, *Microsc. Microanal.* **2014**, *20*, 1764.

Provided by Sächsische Landesbibliothek - Staats- und Universitätsbibliothek Dresden